7

Studies on the Gamma Radiation Responses of High Tc Superconductors

Carlos M. Cruz Inclán, Ibrahin Piñera Hernández,
Antonio Leyva Fabelo and Yamiel Abreu Alfonso
Center of Technological Applications and Nuclear Development, CEADEN
Cuba

1. Introduction

The Future applications of new solid state materials, electronic devices and detectors in radiation environments like Fission and Fusion new generation of Nuclear Reactors, as well as astronomical researches, require a well established understanding about the radiation response of all these items.

In addition to foregoing applications the Gamma Radiation (γR) combined effects of energy dependent displacement per atom (dpa) rates and high penetration strength might be attractive for getting a deeper understanding. In particular for high temperature superconductors (HTS) these are interesting for get a better comprehension about their superconducting mechanisms.

Quite controversial results have been reported in γR damage studies on HTS, especially on regard to the $YBa_2Cu_3O_{7-x}$ (YBCO) superconducting behavior. On this way, the papers dedicated to study gamma irradiation effects on the HTS properties are characterized for a lack of coincidence in criteria and results. Some authors have observed an improvement of the superconducting properties with dose increment (Boiko et at., 1988; Leyva et al., 1992), some others report exactly the opposite (Vasek et al., 1989; Elkholy et al., 1996), and other studies have not found any dependence (Bohandy et al., 1987; Cooksey et al., 1994). These contradictions have not been completely explained yet; some authors even attribute these behaviors to a "sample effect" (Polyak et al., 1990).

However, Belevtsev et al. (Belevtsev et al., 2000) has determined the relationship between the superconducting order parameter ξ_2 and the density of oxygen vacancy rate lower bound, expressed in displacement per atom, in order to achieve significant modification of the superconducting behavior. On this ground, by means of the Oen-Holmes-Cahn atom displacement calculation algorithm (Oen & Holmes, 1959; Cahn, 1959), they calculated the incoming gamma quanta total flux inducing a dpa rate of about 0.02. That makes the $YBa_2Cu_3O_{7-\delta}$ superconducting material mean intervacancies distance close to its superconducting coherence length or order parameter ξ_2, in which case the superconducting properties will be modified.

Consequently, a systematic behavior of HTS material properties upon γR must be expected to be observed, where superconducting intrinsic properties (crystal and electronic structures, critical superconducting temperature), as well extrinsic ones (critical

superconducting electrical current, electric resistivity at normal state) must show proper dependences on both, the induced dpa rates and the gamma radiation incident energies.
Present chapter is devoted presenting the research findings on regard the main physical issues characterizing the gamma radiation damages in high Tc superconductors, focusing to the induced superconducting and normal state physical properties modifications.
Firstly, in section 2 the basic concepts in gamma radiation damage studies on solids are presented, supported by an introduction to main approaches for calculating dpa rate distributions, which are discussed in section 3. Section 4 is devoted to simulations studies of gamma radiation transport in YBCO material, particularly those related to in-depth dpa profile distribution. Gamma radiation damage effects on the YBCO intrinsic properties are reported in section 5, involving the crystalline structure and superconducting critical temperature T_c behaviors under gamma irradiation. Finally, the γR damage effects on the YBCO extrinsic properties on regard to the superconducting critical electric current Jc and electrical resistivity in non superconducting normal state are discussed in section 6.

2. Basic concepts in gamma radiation damage studies on solids

Gamma rays transport in solid matrix involves multiple gamma quanta and secondary electrons interactions with host material valence and core atomic electrons as well with atomic nuclei leading to modifications of its crystal structure by the formation of an amount of point defects, like ionizations, color centers and atom displacements from crystalline sites. These defects modify the irradiated target microscopic and macroscopic properties in a specific way, which is usually referred as Gamma Radiation Damage.
A general measure of all these accounts related to Gamma Radiation Damage is the energy deposition at a given point in the target. Energy deposition spatial distribution can be calculated by means of Monte Carlo assisted gamma quanta transport codes, like EGS-4 (Nelson et al., 1985), EGSnr (Krawrakov & Rogers, 2003) or MCNP (Briesmeister, 2000). Alternatively, for measuring the intensity of the irradiation effects it has been applied the total incident gamma quanta fluence, as well as, the so called exposition doses.
However, from all point defects induced by gamma ray transport in solids, atom displacements might induce a large time scale target properties modification because of the huge time of life of induced vacancies and interstitial Frenkel pairs defect in target crystalline structure. Therefore, gamma radiation damage in solids is commonly described by the spatial dpa distribution. However, because of the insignificant photon transferred energies in their interactions with atoms, secondary electrons must be considered as the unique particles transferring enough recoil energy to the target atoms for leaving their crystalline sites leading to atom displacements processes in solids.
Consequently, high energy secondary electrons induced by gamma ray transport in solids might be considered its main radiation damage source through the basic atom displacements mechanism. This occurs as a result of high transferred recoil energy arising at high scattering angle electronic elastic collision with atoms. This is assumed to be truth whenever $T^k \geq T^k_d$ *(atom displacement main requirement)* (Corbett, 1966). Here T^k is the recoil kinetic energy transferred to the atomic specie A_k placed at a given crystallographic site and T^k_d is the corresponding atom displacement threshold energy value. T^k_d may depend on the crystallographic site and generally ranges between 20 eV to 40 eV. At a given initial electron kinetic energy E_i, T^k will be higher at lower atomic mass M_k and higher scattering angle θ $(\theta \rightarrow \pi)$.

From the atom displacement main requirement, it follows that secondary electrons will induce atom displacements processes through the elastic atomic scattering for $E_i \geq E_C$ (Corbett, 1966; Piñera et al., 2007a), where

$$E_c = \sqrt{(mc^2)^2 + \tfrac{1}{2} M_k c^2 T_d^k} - mc^2 \tag{1}$$

For example, assuming for oxygen $T^O{}_d = 20\ eV$ (Piñera et al., 2007a), then $E_C = 130\ keV$ for oxygen in YBCO. However, for the O(5) YBCO crystalline sites, at the Cu-O chains at the crystal cell basis plane, Bourdillon & Tan had reported $T_d{}^{O(5)} = 3.45\ eV$, leading to a $E_c(O(5)) = 26\ keV$ (Bourdillon & Tan, 1995)**.**

The removed atom as a result of an electron elastic atomic scattering is known as Primary Knock-on Atom (PKA). If any of these recoil atoms has a kinetic energy above the displacement threshold energy *Td*, the secondary atoms can be knocked-on by PKA and additional dpa cascades can be ascribed to the corresponding displaced atoms. Thus, these secondary atoms will enhance dpa rates on regard to PKA ones with an increasing contribution whenever $\boldsymbol{T^k \gg T^k_d}$.

Threshold energy $\boldsymbol{T^k_d}$ could be experimentally determined by high energy electron microscopy (over 200 keV), where the irradiating electron beam is applied for both, inducing and detecting vacancies when the electron beam incident energies is over $\boldsymbol{E_c}$ (Kirk et al. 1988; Frischherz, 1993; Kirk & Yan, 1999). Alternatively, spectroscopic methods like Electron Paramagnetic Resonance (EPR) and Hyperfine Interaction Methods may be applied indirectly for these purposes, by analyzing "off beam" electron or gamma quanta irradiated samples, searching for evidences of vacancies or other point defects induced on this way (Lancaster, 1973; Jin et al., 1997). The application of Mössbauer Spectroscopy in this framework is presented in section 5.1. For high symmetric and simple crystalline structures, like TiO_2, theoretical methods had been applying for threshold energy $\boldsymbol{T^k_d}$ determination, mainly through the application of the Molecular Dynamic approaches (Thomas et al., 2005).

3. Main approaches for calculating atom displacements rate distributions

3.1 Averaging methods following Oen – Holmes – Cahn algorithm

The mean number of electron elastic atomic scattering events leading to atom displacements processes along a given electron path can be calculated according to the expression

$$n_{dpa} = \sum\nolimits_{k,i} N^{e,k}_{dpa,i} = \sum\nolimits_{k,i} N^k_i \sigma^k_{dpa}(E_i) \Delta S_i \tag{2}$$

where $N^{e,k}_{dpa,i}$ is the number of atom displacements processes induced in a sectional electron path length ΔS_i, σ^k_{dpa} is the total electron elastic atomic scattering cross section (enhanced by the atom displacements contribution of secondary atoms ejected by PKA) ascribed to the k-th atomic specie with atomic density N^k_i for electron initial energies E_i at the beginning of the i-th sectional path, where it is assumed that $\sigma^k_{dpa}(E_i) = 0$ for $E_i \leq E^k_c$. In Fig. 1 is schematically represented a secondary electron scattering path.

Oen, Holmes and Cahn (Oen & Holmes, 1959; Cahn, 1959) had applied Eq. (2) by approaching the electron kinetic energy values at a given section path E_i as a continuous function of path length *S*,

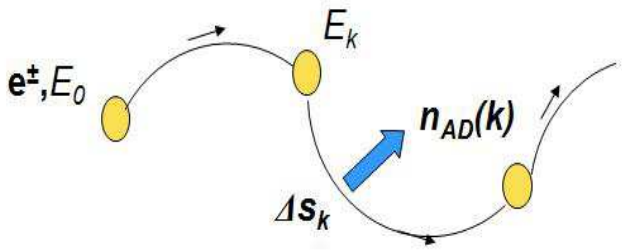

Fig. 1. A simplified physical picture of the electron transport in a solid matrix. Smooth movements along continuous path sections mostly prevail, representing an averaged multiple scattering events under low transferred energy and linear momentum values. These continuous sections delimited by single point like scattering events, where the electrons may suddenly change their kinetic energy and linear momentum values.

$$E(S) - E(0) = \int_0^S \left(-\frac{dE}{ds} \right) ds \tag{3}$$

where $\left(-\frac{dE}{ds} \right)$ is calculated following standard electron linear energy loss formula, as for example Bethe – Ashkin equation (Bethe & Ashkin, 1953), which represents a smoothed picture of the real fluctuating nature of high energy electron movements in a solid. Consequently, Eq.(2) is approached as

$$N_{dpa}^{e,k} = N_a \int_{E_c^k}^{E} \sigma_{dpa}^{k}(E(s'))ds' = N_a \int_{E_c^k}^{E} \frac{\sigma_{dpa}^{k}(E')}{\left(-\frac{dE}{ds'} \right)} dE' \tag{4}$$

where N_a is the number of atoms in the unit volume in the sample. Then, by assuming a mean energetic electron flux distribution $\Phi(E_i,z)$ in the neighborhood of a target sample point at a depth z, the Oen-Homes-Cahn algorithm calculates total number of displacement per atom N_{dpa} at the given point according to the expression

$$N_{dpa} = \sum_k \left(n_k \left(\sum_i N_{dpa,k}^{e}(E_i)\Phi(E_i,z)\Delta E_i \right) \right) \tag{5}$$

where n_k denotes the relative fraction of the *k*-atom in its crystalline sublattice. The Oen-Holmes-Cahn algorithm will be referred as the "atom displacements Classical Method calculation".

The applications of the Eq. (5) in the practice have been done mostly assuming a "model" dependence $\Phi(E_i,z)$ following an in depth exponential decay law as well as the Klein - Nishina energy distribution for electron emerging from a Compton interaction. This approach was applied by Belevtsev et al. to YBCO dpa calculations (Belevtsev et al., 2000). However, Piñera et al. had shown by means of Monte Carlo Methods assisted gamma quanta transport calculations in YBCO matrix, that $\Phi(E_i, z)$ does not follow such a "model" dependence on regard of both, E_i *and* z as it is shown in Fig. 2 (Piñera et al., 2007a).

In Fig.2 the kinetic energy distribution of electrons energy fluxes were calculated for YBCO ceramic sample with parallelepiped form. These distributions were determined in the central line voxel at a depth corresponding to the maximum energy deposition on which impact photons at different selected incident gamma energies. Monte Carlo method code MCNP-4C was used.

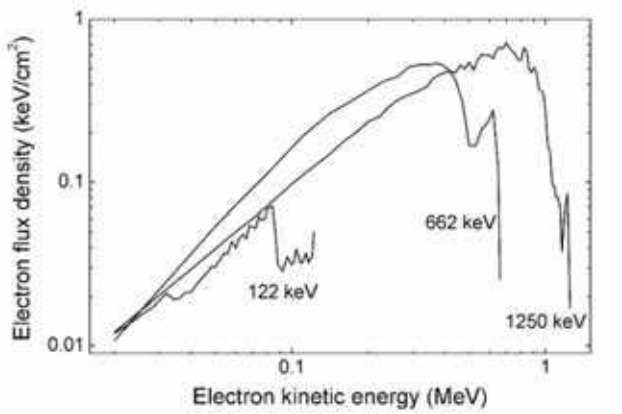

Fig. 2. Kinetic energy distribution of electrons energy flux in central voxel for different incident gamma energies. (Piñera et al., 2007a)

Two important facts arise from these kinetic energy distribution profiles $\Phi(E_i,z)$. Firstly, the ejected photoelectrons own the higher kinetic energies values ($\approx E_\gamma$) with an appreciable relative intensity, which can give an important contribution to dpa rate. On the second place, the continuous Compton electron contribution at lower energies becomes a broader unimodal distribution with a relative maximum near to the Compton electron maximum kinetic energy. This is an essentially different behavior, as predicted by Klein-Nishina scattering law for Compton scattered electrons ruled by electron multiple scattering relaxation processes (Klein & Nishina, 1929).

Therefore, this complex electron kinetic energy distribution behaviors seen before do not agreed with the starting assumptions taken in by Belevtsev et al. for the direct calculation of dpa rate in YBCO (Belevtsev et al., 2000), clearly supporting the introduction of a more realistic treatment for secondary electron transport as done in Monte Carlo based codes here applied. This is the aim of the Monte Carlo assisted Classical Method (MCCM) introduced by I. Piñera et al. (Piñera et al., 2007a, 2007b, 2008a, 2008b).

The MCCM consists in applying to the classical theories about atom displacements by electrons and positrons elastic scattering with atoms the flux $\Phi(E_i,z)$ distribution of these particles obtained from the Monte Carlo simulation. Oen-Holmes-Cahn Classical Method does not take into account the shower and cross linked nature of the gamma quanta and the secondary electron interactions happen at γR transport in solids. But this γR complex stochastic behavior can be nowadays very well simulated and described through calculation codes based on Monte Carlo method, modeling the transport of different types of radiations in substance. Thus, on this basis, it can be locally calculated the Energy Deposition distribution as well as the energy profile flux distributions of the transported particles, which might provide the calculation tools required for Radiation Damage evaluation.

By the application of Eq. (4) in MCCM,

$$\sigma_{dpa}^{k}(E) = \sigma_{PKA}^{k}(E) \cdot \nu(T) \tag{6}$$

where $\sigma_{PKA}^{k}(E)$ is the PKA cross section following the McKinley – Feshbach equation (McKinley & Feshbach, 1948)

$$\sigma_{PKA}^{k}(E) = \frac{\pi r_0^2 Z_k^2}{\beta^4 \gamma^2} \cdot \{\tau - 1 - \beta^2 \ln(\tau) \pm \pi\alpha\beta\left[2\sqrt{\tau} - \ln(\tau) - 2\right]\} \tag{7}$$

with Z_k being the atomic number of the k-atom, r_0 is the electron classic radius, $\alpha = Z_k/137$, $\boldsymbol{\beta}$ is the ratio of the electron velocity to the velocity of light, $\boldsymbol{\gamma}^2 = 1/(1 - \beta^2)$, $\boldsymbol{\pi} = T^k_{max}/T^k_d$, being $T^k_{max} = 2E(E + 2mc^2)/M_k c^2$ the maximum kinetic energy of the corresponding recoil atom with mass M_k and $\nu(T)$ is the damage function, which in the case of MCCM is implemented according to the Kinchin – Pease model (Khinchin & Pease, 1955)

$$\nu(T) = \begin{cases} 0, & T < T_d^k \\ 1, & T_d^k \le T \le 2T_d^k \\ \frac{T}{2T_d^k}, & T > 2T_d^k \end{cases} \tag{8}$$

This damage function introduces an enhancement factor in dpa calculations due to the atom displacement cascades phenomenon. To evaluate $\nu(T)$ in MCCM, the average value of the scattered atoms energies, $\boldsymbol{T}^k_{ave}$, is calculated through the expression

$$T_{ave}^{k} = \frac{\tau\ln(\tau) - \beta^2(\tau-1) \pm \pi\alpha\beta(1-\sqrt{\tau})^2}{\tau - 1 - \beta^2\ln(\tau) \pm \pi\alpha\beta\left[2\sqrt{\tau} - \ln(\tau) - 2\right]} \tag{9}$$

3.2 Monte Carlo Simulation of Atom Displacements

The basic ideas supporting the present description of the atom displacements processes induced by the electron transport in a solid matrix are represented in Fig. 3. As usually, in a macroscopic scale, the Monte Carlo Methods based simulation of the electron transport in solids is treated as a sectional smooth continuous path, delimited by discreet point like events arising at high transferred energy and linear momentum. In the present case, the atom displacements processes are only produced at elastic scattering discreet events at high scattering angles, where enough energy is transferred to an atom to be ejected from its crystalline site. It will also imply that atom displacements processes do not take place under the sectional continuous path.

As a reference point, in Fig. 3 is also represented the Fukuya's approach to atom displacements processes (Fukuya & Kimura, 2003), following the classical Oen-Holmes-Cahn dpa calculation algorithm. In this case, the continuous electron motion path lengths are sampled according to a Monte Carlo simulation of the gamma quanta and electron transport in a solid under which the electron elastic scattering events at high scattering angles are not involved. Consequently, atom displacements processes are essentially

calculated in Fukuya's approach on the basis of the continuous path lengths which really are connected to an averaged multiple quasi-continuous electron motions under small electron linear momentum and energy instantaneous changes.

Cruz et al. proposed a new approach involving the full Monte Carlo Simulation of Atom Displacements (MCSAD). In MCSAD the occurrence of single and multiple Elastic Scattering (ES) events is defined by the limiting scattering angle θ_l, according to Mott's criteria (Mott & Massey, 1952), at which the electron single and multiple ES probabilities become equals.

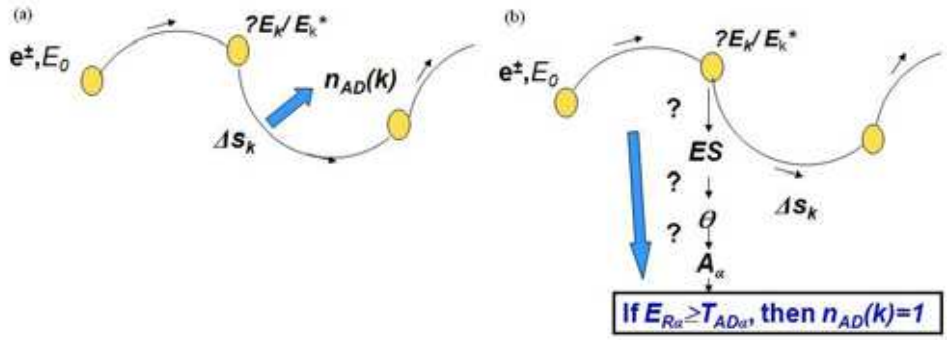

Fig. 3. (a) Fukuya's treatment of atom displacements processes (Fukuya & Kimura, 2003). (b) New MCSAD approach (Cruz et al., 2008). E_k denotes the electron kinetic energy; n_{dpa} is the number of atom displacements events. Solid bold balls represent the occurrence of single scattering events (Elastic Scattering, Moeller or Bremsstrahlung).

Electron multiple ES probability were calculated according to Moliere-Bethe Theory (Bethe, 1953). Thus, McKinley-Feshbach cross section was renormalized for the occurrence of single ES between π and θ_l according to the following expression for the total Macroscopic Cross Section $\Sigma_{ES}(\theta_l)$ of the discreet electron elastic atomic scattering processes

$$\sum_{ES}(\theta_i)=\frac{1}{4}\frac{\theta_c^2}{\Delta s}\xi^{-2}\left[1\pm 2Z\pi\alpha\beta\xi\right]-(1\pm 2Z\pi\alpha\beta)\xi^2+2\left(\beta^2\pm Z\pi\alpha\beta\right)\xi^2\ln(\xi) \qquad (10)$$

where $\xi=\sin(\theta_1/2)$, $\beta=(1-E_0^2/E^2)$, $\theta_c^2=(0.60089)Z_s(\frac{\rho\Delta s}{A})(\frac{c^2p^2}{E})^2$ and Z_s is defined in the EGS-4 user manual (Nelson et al., 1985). The positive sign is related to the electron scattering and the negative sign to the positron one.

The occurrence of an electron single ES event is sampled regarding the other competing interactions (Moeller electron scattering, Bremsstrahlung and Positron Annihilation). The emerging electron single ES angular distribution was described applying the McKinley – Feshbach cross section formula restricted to the scattering angles inside the interval $\theta_l \le \theta \le \pi$, which was consequently renormalized by the Total Macroscopic Cross Section $\Sigma_{ES}(\theta_l)$ value given by Eq. (10). This angular probabilistic distribution function was statistically sampled by the application of the combination and rejection methods.

On this way ES scattering angle θ was sampled and the occurrence of this event at a given constituting atom A_k will randomly arise by taking into the account to the relative weight of each atomic species in the total elastic scattering process. Consequently, a given atomic sort

A_k is sampled and the transferred energy T^k is determined. Following the atom displacement main request, if $T^k \geq T^k_d$ hold for the stochastically chosen k-th atomic specie, then $n_{dpa} = 1$, which means that an atom displacement event takes place. Otherwise, single ES event leads to a phononic excitation of the solid.
Some partial results involving Monte Carlo gamma quanta and secondary electron simulations on regard atom displacements rates produced in YBCO are represented in Fig. 4 for different electrons initial energies. Fig. 4 shows that each atomic specie contributes to atom displacement processes only over a given critical electron kinetic energy E_c. A critical evaluation among MCSAD predictions with those previously obtained by Piñera et al. and Fukuya-Kimura is in course (Piñera et al., 2007a, 2007b, 2008a, 2008b; Fukuya & Kimura, 2003).

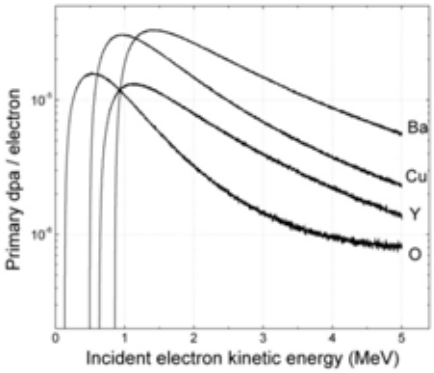

Fig. 4. Monte Carlo simulation of ES processes inducing Primary Knock-On Atomic Displacements in $YBa_2Cu_3O_{7-\delta}$ depending on electron initial energy at a given discreet event.

4. Monte Carlo numerical simulations of gamma radiation damage in YBCO

4.1 Gamma ray dpa in-depth distribution in YBCO

Some results of applying MCCM method on slab samples of the YBCO superconducting material are reported here. The MCNPX code (Hendricks et al., 2006) was used for simulation purposes, considering that it gives directly the flux energy distribution through its energy bin *F4 tally, separating contributions from electrons and positrons with the help of the FT card ELC option. Fig. 5 shows the calculated number of displacement per atom for electrons and positrons for incident gamma energies (E_γ) up to 10 MeV.
As it can easily observed, the shape of these profiles for electrons and positrons are very similar. Also, the *dpa* values are always higher at higher incident radiation energies in all the sample volume and the damage increases drastically with depth as the incident energy increases. Also, averaging the $N_{dpa}(z)$ values over the sample thickness, the total *dpa* for each E_γ is obtained. This was done in such a way that we could evaluate separate the contributions from electrons and positrons. These contributions are shown in Fig. 6a together with the total *dpa* distribution.
As can be seen from this figure, the contribution from electrons to the total *dpa* is greater up to about 8 MeV, beyond which the *dpa* induced by positrons begins to prevail. At E_γ = 10 MeV the positrons *dpa* contribute for 53.4%, almost 7% higher than the corresponding contribution induced by electrons. It is important to note that, when positrons are also

considered in the atom displacement process, the total *dpa* at 10 MeV of incident gamma radiation increase up to 2.15 times compared to the situation that only electron interactions are considered. The contribution from each atom to the total *dpa* value was also possible to be studied like it is shown in Fig. 6b. The contribution of the Cu-O_2 planes was considered, taking together the effects on the oxygen and the copper atoms in those sites. The results show that the contribution to the total damage from yttrium and barium atoms is smaller than the contribution from the Cu-O_2 planes. They have a maximum contribution of 11.7% (in case of Y) and 30.9% (in case of Ba) for 10 MeV of incident radiation. This result could support the fact that Y and Ba displacements are not decisive for the possible changes provoked in this material at low and medium energies (Belevtsev et al., 2000; Legris et al., 1993). Then, the main contribution to the total damage comes from the Cu-O_2 planar sites in the sample in the studied energy range.

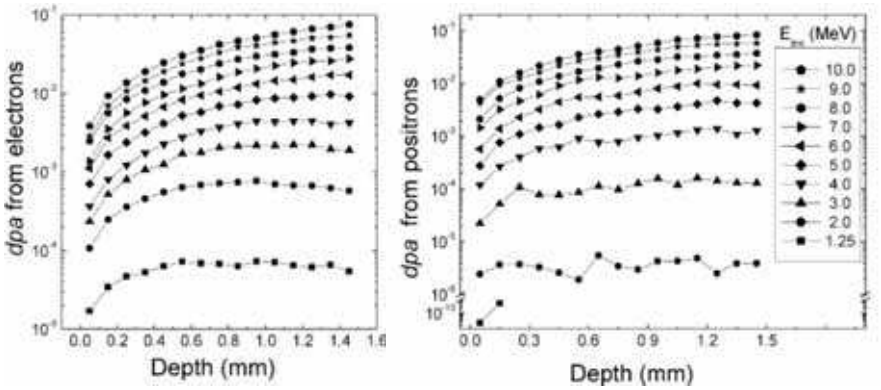

Fig. 5. *dpa* in-depth distributions due to electrons (left) and positrons (right) for different incident energies. Continuous lines are only visual guides.

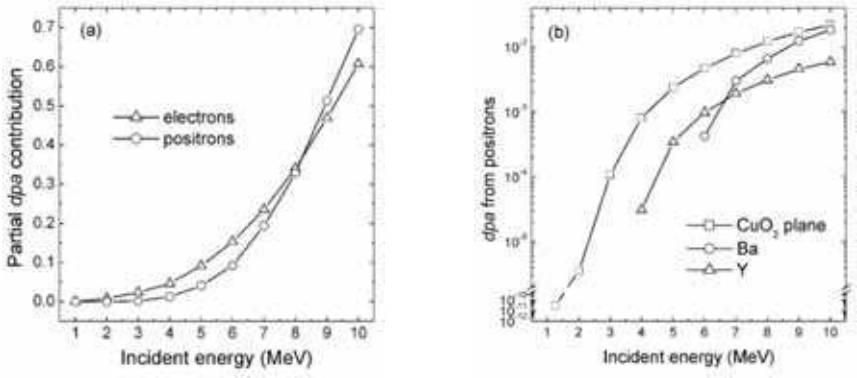

Fig. 6. (a) Number of *dpa* induced by electrons and positrons at different incident gamma energies. (b) Number of positrons *dpa* corresponding to each atom site at different incident gamma energies. All continuous lines are only visual guides.

The independent contributions from oxygen and copper atoms to the in-plane dpa could be also analyzed. The contribution from oxygen atoms diminishes with increasing the incident

energy while the contribution from copper atoms increases to 62% in the studied energy range. Another interesting observation is that the main dpa contribution with regard to the Cu-O_2 planes arises from O-displacements up to 4 MeV. But at higher energies, an increasing role of Cu-displacements is observed, reaching a maximum contribution of about 65% inside planes at E_γ = 10 MeV (Piñera et al., 2008a).
Similar analysis about these points can be made taking separately the contributions from positrons and electrons.

4.2 Dependency between dpa and energy deposition

Comparing the dpa distributions from Fig. 5 with the corresponding energy deposition profiles and taking some previous own-works as reference, was possible to study the dependence between both distributions (dpa and energy deposition), like that shown in Fig. 7a. It seems apparent from this figure that a nearly linear dependence may be established between the energy deposition and the number of atoms displaced by the gamma radiation at a given incident energy in the YBCO material. For this reason we carry out the linear fitting of these dependences, which can be analyzed in Fig. 7b, obtaining the dpa to energy deposition production rate η at each incident energy. Correspondingly, it can also be asserted that the Gamma Radiation energy deposition process in YBCO material supports better the atom displacement production at higher incident energies.

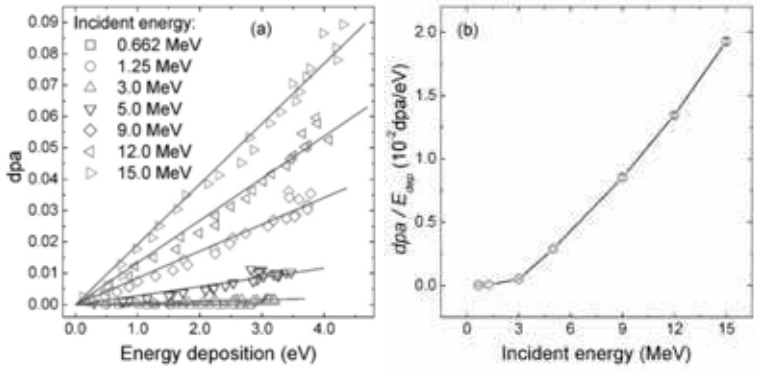

Fig. 7. (a) Dependence between dpa and energy deposition for each incident energy. Continuous lines represent the linear fitting. (b) Displacements to energy deposition rate as function of the incident energy. Continuous lines are visual guides.

Consequently, there exists a general local dependence among N_{dpa} and E_{dep} values, independently of the given target position,

$$N_{dpa} = \eta(E_\gamma) \cdot E_{dep} \tag{11}$$

where η is the dpa rate per deposited energy unit at any target position, which depends on the initial gamma ray value following Fig. 7b, as well as on the atomic composition of the target material (Piñera, 2006).
These particular behaviors should be expected, since secondary electrons play an important and decisive role on the general energy deposition mechanism and particularly on displacing atoms from their crystalline sites. On this basis, it must be reasonably to assume

that the previously findings reported by Leyva (Leyva, 2002) (see below section 5.2) on regard with the observed correlation among in-depth measured T_c and calculated E_{dep} values might be extrapolated to among the former one and the calculated dpa values.
On the other hand, exposition doses D_{exp}, is related to the total incident gamma ray quanta through the equation

$$\Phi = \frac{D_{\exp}}{E_\gamma} \cdot \frac{\rho_{air}}{\mu_a(E_\gamma)}, \tag{12}$$

where $\mu_a(E_\gamma)$ is the gamma air mass absorption coefficient at the incident energy E_γ and Φ is the incoming total gamma quanta. On this way, knowing the exposition dose D_{exp} from dosimetric measurements, Eq. (11) allows to calculate Φ. This is related with the number of histories of independent gamma ray transport to be calculated by means of any of the Monte Carlo based codes introduced above in sections 2 and 3. Then, E_{dep} and N_{dpa} distributions corresponding to a given irradiation experiment can be determined through theses D_{exp} values.

5. Gamma radiation damage effects on the YBCO intrinsic properties: crystalline structure and superconducting critical temperature T_c

5.1 Gamma ray influence on YBCO crystalline structure

The ideal well ordered orthorhombic $YBa_2Cu_3O_{7-x}$ unit crystal cell owing high Tc superconducting behaviour (Fig. 8a) is observed only for $\delta \leq 0.35$, where Oxygen site O(5) along the a axis are completely unoccupied (Santoro, 1991). For $\delta \geq 0.35$ this material undergoes an orthorhombic to tetragonal phase transition, which is shown in Fig. 8b through the temperature behavior by heating of the $YBa_2Cu_3O_{7-\delta}$ orthorhombicity parameter (ε), where $\varepsilon = (a-b)/(b+a)$. It is observed that at 950 K, $\varepsilon = 0$, which means that lattice constants *a* and *b* become equals, which corresponds to the tetragonal crystal structure.

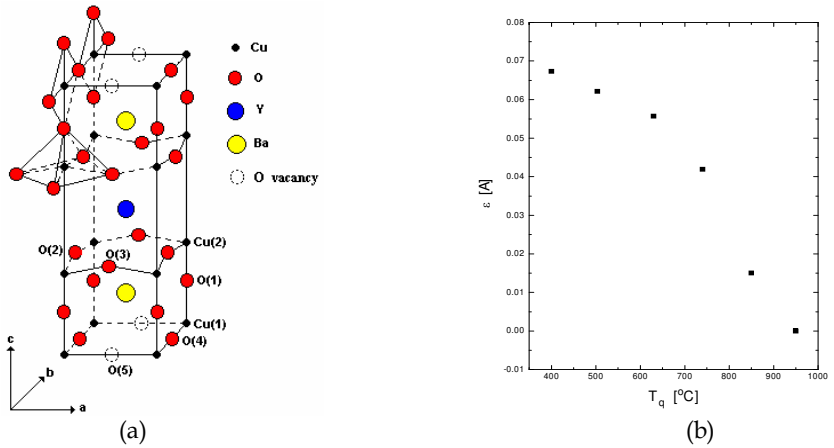

(a) (b)

Fig. 8. (a) YBCO orthorhombic crystal unit cell. (b) YBCO orthorhombicity temperature dependence.

In connection with YBCO crystal structure featuring, Cu(1)-O chains in the basal planes play an important role, since its YBCO non–stoichiometric behavior is related to existing Oxygen vacancies in these sites (O(4)). It modulates also its electrical conducting properties (Gupta & Gupta, 1991) for $\delta \leq 0.35$ it owns metallic conduction (it turns superconducting at $T \leq T_c$), while for $\delta \geq 0.35$ it reaches a semiconducting behavior, being the electronic conduction associated to Cu(2) – O_2 planes.

Though an ideal orthorhombic structure is accepted to be observed at $\delta = 0$, for $\delta > 0$ an $YBa_2Cu_3O_{7-\delta}$ oxygen disorder at its crystal unit cell basis plane take place: both, O(4) and O(5) sites, are partially and random occupies. Therefore, Cu(1) sites will be surrounded by different oxygen configurations, where the four neighbor oxygen positions O(4) and O(5) will be randomly occupied.

Fig. 9 shows the different oxygen nearest neighborhood around the Cu(1) sites, where the nomenclature OC. Nα idicates the oxygen coordination number N, oriented in the α direction. At the orthorhombic structure, $0 < \delta \leq 0.35$, O(4) sites will be preferably occupied, oxygen rich nearest neighbor configurations OC.4α, OC.4αβ, OC.5α are mostly to be expected. X- Ray Diffraction studies had shown the tendency, that higher O(4) occupation fraction leads to shorter Cu(1)-O(4) distance, while lower O(5) occupation fraction leads to higher Cu(1)-O(5) distance. On the contrary, at the tetragonal structure, $\delta > 0.35$, both, O(4) and O(5), are randomly, but equally occupied, pour oxygen nearest neighbor configuration only take place. In the limit of $\delta = 1$, which observed at annealing temperature over 1200 K, both oxygen basal plane positions remain unoccupied. The ordering of the atoms of oxygen in the chains plays an important role in the control of the charge carrier concentration in the CuO_2 planes (Gupta & Gupta, 1991), what must influence the superconducting intrinsic properties, like Tc.

YBCO samples exposed to ^{60}Co gamma irradiation does not follow the orthorhombic to tetragonal structural transition pattern observed by heating, as it can be easily observed by comparison of the ε orthorhombicity parameter behaviors shown in Figs. 8b and 10b.

YBCO samples were irradiated in a ^{60}Co gamma chamber and the orthorhombic lattice constants were measured by X-Ray Diffraction. The dose dependence of the experimentally determined lattice constants for one representative sample is shown in Fig. 10a. The values corresponding to the YBCO cell parameter obtained from (JCPDS, 1993) have been represented by dashed lines and will ascribed as YBCO ideal structure parameters with optimum superconducting properties.

The sample just after the synthesis process presents oxygen basal plane disorder in its structure as a result of the heat treatments, since its lattice parameters were found away from the ideal ones. With the beginning of the irradiation process a singular behavior of the lattice parameters is observed (see Fig. 10a). The *b* and *c* reach their optimum values at near the exposition dose $E_0 \approx 120$ kGy, beyond E_0 they diminish approaching to some intermediate value between the optimum and the initial ones. The lattice constant a changes monotonically, approaching for $E_{dose} \geq E_0$ to its optimum value. On the other hand, the orthorhombicity parameter ε oscillates around the YBCO optimum value.

It is clear from the lattice constants and crystal cell parameters behaviors under gamma irradiation shown in Fig. 10, that gamma ray induced YBCO crystal structure variations do not correspond to a deoxygenating process, as in thermal activated treatments at temperatures higher than 600 K, in which cases the non – stoichiometric parameter δ increases, provoking the $YBa_2Cu_3O_{7-\delta}$ orthorhombic to tetragonal phase transition. In any

case, it seems that the gamma exposition, specially at doses about E_0, has stimulated an population increase of the oxygen rich nearest neighbor configurations in the oxygen basis plane disorder picture , like the OC.4α, OC.4αβ, OC.5a ones, as it is expected from the a and b approaching tendency to $YBa_2Cu_3O_{7-\delta}$ ideal crystal structure values. At higher exposition doses, it seems that the oxygen rich nearest neighbor configuration population displace partially back from the optimum ones and tend to stabilize to a long range orthorhombic structure.

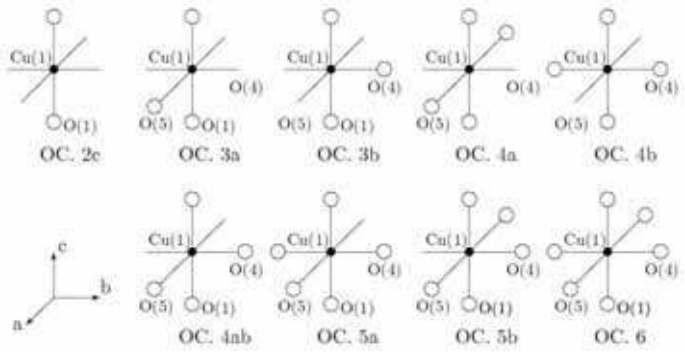

Fig. 9. Oxygen configurations (OC) formation considered around Cu(1) position.

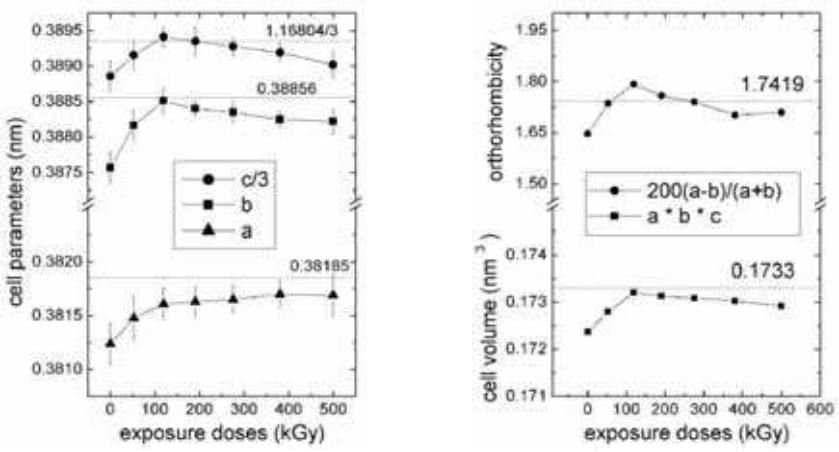

(a) (b)

Fig. 10. ^{60}Co - γ dose exposition dependence of the YBCO elementary cell parameters, volume and orthorhombicity behaviors measured by X-Ray Diffraction. (a) Orthorhombic cell lengths a, b and c. (b) Elementary volume and orthorhombicity. Dashed lines represent the presupposed optimum values of YBCO cell parameters, volume and orthorhombicity.

It is possible to get deeper in the foregoing gamma radiation damage picture by means of the application of the magnetic resonance methods and the hyperfine interaction techniques, like the Mössbauer Spectroscopy, allowing a better understanding of the crystal short range order, especially defects properties, since in X-ray Diffraction studies long range crystal order is better evaluated. Therefore the gamma radiation impact on YBCO oxygen basis

plane disorder had been studied by ^{57}Fe Mössbauer Spectroscopy (Jin et al., 1997), in which case, ^{57}Fe very low doping contents were applied ($YBa_2(Cu_{0.97}Fe_{0.03})_3O_{7-\delta}$) and the Fe: YBCO doped samples were exposed with ^{60}Co gamma radiation up to 1 MGy.
The Mössbauer spectra were measured after and before irradiation; these spectra are characterized by four lines presented in Table 2; and the main effect they observe was that the D1 doublet relative area decreases and the D4 doublet relative area increases in correspondence. The variation on these magnitudes was around 5% and the created damage was reversible after some days. This radiation effects were ascribed to some oxygen coordination environment associated to D1, which becomes under irradiation in some other one related to D4 due to mainly atoms displacements and electron trapped in vacancies (color centers). This effect is different from the one observed by thermal activation oxygen hopping between the coordination structures of doublets D1 and D2 (Jin et al., 1997).

Doublet	IS (mm/s)	ΔE_Q (mm/s)	W (mm/s)	S (%)
D1	0.06	2.00	0.16	32
D2	0.03	1.10	0.25	53
D3	0.23	0.40	0.16	12.2
D4	0.24	0.16	0.10	4.8

Table 2. Isomer shift (IS), quadruple splitting (ΔE_Q), line width (W) and relative area (S) of ^{57}Fe subspectra in the Mössbauer spectra of $YBa_2(Cu_{0.97}Fe_{0.03})_3O_{7-\delta}$ samples (Jin et al., 1997).

To analyze these observations the correspondence between ^{57}Fe crystallographic sites and the Mössbauer subspectra should be take in to account; but some contradictions subsist in the interpretation of ^{57}Fe Mössbauer spectra in $YBa_2Cu_3O_{7-\delta}$ (Jin et al., 1997; Boolchand & McDaniel, 1992; Sarkar et al., 2001; Liu et al., 2005), reason that stimulated the reanalysis of this problem. In order to promote these aspects, a methodology developed by Abreu et al. (Abreu et al., 2009) was used to consider the structural defects influence in the quadruple splitting observed values; through the calculation of the electric field gradient (EFG) components in this situation by the point charge model (Abreu et al., 2009; Lyubutin et al., 1989). Specifically the point defects are taken in to consideration through different oxygen configurations, like cluster formation around the ^{57}Fe position and vacancies; and electron trapped in vacancies near this position too, like negative vacancies.
To take in to consideration the influence of crystallographic point defects in the Mössbauer probe atom neighborhood to the EFG, the methodology presented by Abreu et al. was applied (Abreu et al., 2009). The EFG values in the material with presence of vacancies and defects (V_{def}) could be consider as the ideal value (V_{ideal}), calculated following the point charge algorithm outside the first coordination sphere where the ^{57}Fe provoke the presence of oxygen atoms over the ideal composition; adding (V_{oc}), which is the EFG value inside the first coordination sphere, considering the formation of oxygen configurations (OC) due to the ^{57}Fe presence in the structure and the radiation damage process (Santoro, 1991).

$$V_{def} = V_{ideal} + V_{oc} \tag{13}$$

Parameters reported for the YBCO (Liu et al., 2005; Lyubutin et al., 1989; Santoro, 1991) were used to calculation the EFG values for the ideal tetragonal and orthorhombic structure. These calculations were made following point charge model algorithm; reaching a precision order in the sum of 10^{-6} for the atoms located inside a sphere with radius R = 380 A^o. The

ionic charges were taken mainly as nominal values: Y^{+3}, Ba^{+2}, O^{-2}, Cu^{+2} for Cu(2) positions; and in the Cu(1) position, Cu^{+1} for the tetragonal case and Cu^{+3} for the orthorhombic ones.
Since the interest is to evaluate the EFG and the corresponding ΔE_Q observed in the Mössbauer experiments of this superconducting material, the ^{57}Fe location will be consider only in the Cu(1) position as it was reported for doublets D1 and D4 (Jin et al., 1997; Boolchand & McDaniel, 1992; Santoro, 1991).
It is also interesting to analyze the influence of Iron atoms introduction in the $YBa_2Cu_3O_{7-\delta}$ crystalline structure. Santoro reported that in that case the oxygen content on the material is over ($7 - \delta \geq 7$); caused by oxygen vacancies population around the Cu(1) position, depending on iron ionization state (Santoro, 1991). For this reason the OC around the Cu(1) position shown in Fig. 9 were considered in the calculations.
Finally, it becomes necessary to obtain the corresponding splitting values due to the hyperfine quadruple interaction of the nuclear sublevels ΔE_Q, which are observed in the experiment. This magnitude could be calculated from the following expression (Abreu et al., 2009; Lyubutin et al., 1989)

$$\Delta E_Q = \frac{1}{2} e V_{zz} Q (1 - \gamma_\infty) \left[1 + \frac{1}{3} \eta^2 \right]^{\frac{1}{2}} \tag{14}$$

where e is the electron charge, Q is the nuclear quadruple momentum of Iron and $1 - \gamma_\infty$ is the Sternheimer anti-shielding factor. To evaluate ΔE_Q the following values of this parameters for the ^{57}Fe (I = 3/2) were used in all cases, Q = 0.16b and γ_∞ = −9.14 (Abreu et al., 2009; Lyubutin et al., 1989).
The calculation results are presented in Fig. 11 for all the oxygen configurations studied. From the ΔE_Q results could be assigned the doublet D1 to the OC. 5a for the orthorhombic structure and OC. 5a & 5b for the tetragonal, while the doublet D4 could be assigned to OC 6. Is clear from these assignations that an oxygen displacement event could move this atom to the vacant position present in the OC. 5; transforming it in the OC. 6. A negative vacancy (electron trapped) was also added to the OC. 5; and in both cases the ΔE_Q values changes as indicated by the vertical arrows; so the same effect is observed with negative vacancies and with oxygen atoms displacements events in the Cu(1) position first coordination neighborhood. With the obtained results the damage effects reported by (Jin et al., 1997) are confirmed. These findings agreed well with those previously reported X-ray Diffraction ones.
X-Ray Diffraction and Mössbauer Spectroscopy studies on ^{60}Co – γ quanta irradiated YBCO samples lead to the conclusion, that gamma radiation induced oxygen displacements in both, Cu(2)-O_2 planes and Cu(1)-O chains (Piñera et al., 2007a), as well as secondary electrons are eventually trapped in unoccupied O(4) and O(5) sites in crystal unit cell basis plane, provoking a strengthening of the orthorhombic structural phase, specially at relative low exposition dose E_0 ≈120 kGy.

5.2 Superconductive critical temperature Tc behavior on the gamma quanta exposition doses

The ^{60}Co-γ radiation induced reinforcement of the orthorhombic crystal structure properties at relative low exposition doses seems to correspond also to an enhancement of the YBCO superconducting properties. A maximum in the T_{on} with the dose dependence for YBCO and BSCCO samples was reported at $E_0 \sim 100$ *KGy* (Leyva et al., 1992). Upon irradiating thick YBCO films, a maximum in the dependence of T_c with E_0 ranging between 120-130 kGy was also observed (Leyva et al., 1995).

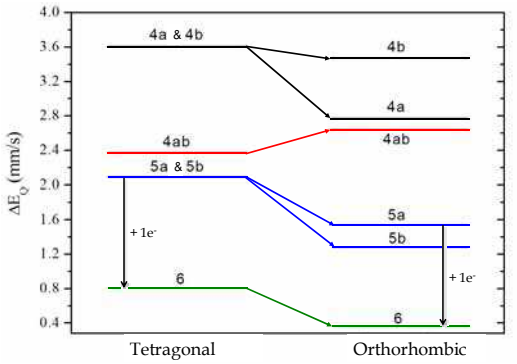

Fig. 11. ΔE_Q values obtained for the OC in the studied crystalline structures.

In Fig. 12 is schematically represented a ^{137}Cs gamma irradiation experiment on YBCO samples, where in depth Tc was measured at defoliated samples after irradiation, as it is shown in Fig. 13a.

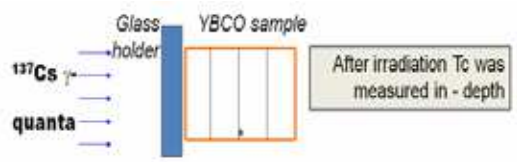

Fig. 12. ^{137}Cs gamma ray irradiation experimental and simulation applied for gamma radiation damage YBCO in depth studies.

The intact samples were placed within a glass container to preserve it from ambient conditions. The container was directly exposed to a ^{137}Cs source calibrated to a power dose of $1x10^{-3}$ Gyh^{-1} until a 0.265 Gy exposition dose was reached. The irradiation took place at room temperature.

For all samples, the transition temperatures were measured using the "four probe method", first placing the probes on the surface that later should be directly exposed to the radiation source and next on the opposite side.

Fig. 13a shows the results of the after irradiation measurements for one representative sample. Measurements made on the surface directly exposed to the source show an improvement of the superconducting properties. Its critical temperature increased in 2.24 K and the transition width decreased from 3.15 K to 1.44 K. The transition temperature values measured on the opposite surface practically did not change.

The in-depth gamma ray energy deposition profile were simulated by means of EGS-4 code, where in the simulation the real geometrical conditions were preserved and $1x10^8$ incidents 662 keV photons were taken in order to obtain a good statistics. The variance of each obtained value did not surpass 0.5 %.

The results of this experiment are very important, showing a positive correlation among in depth T_c measured values with the simulated deposited energy ones, as an increasing monotonic "*in situ*" relationship, since in previous gamma ray induced Tc enhancement reports, Tc were measured only on the irradiated sample surface and global irradiation effects by means of the exposition doses measurements were established. Furthermore, the Eq. (11) lead also to the conclusion, that such an in-depth correlation among Tc and the

energy deposition values must be worth among the former ones and the atom displacement rate N_{dpa}. This means that the upraise of induced vacancy concentration (relaying mainly for ^{137}Cs in changes in the oxygen distribution in YBCO basal plane) at the YBCO incident surface provokes a Tc increase, very close to the above reported ^{60}Co-γ radiation YBCO Tc enhancement and in excellent agreement with X-Ray Diffraction and Mössbauer Spectroscopy findings seen in section 5.1.

However, this YBCO Tc gamma radiation induced enhancement depends on the initial non-stoichiometric parameter δ (Leyva, 2002), as it is shown in Fig. 14. Here, YBCO samples with different non-stoichiometric parameter δ (and corresponding different initial Tc values) were irradiated with ^{60}Co gamma ray at different exposition doses.

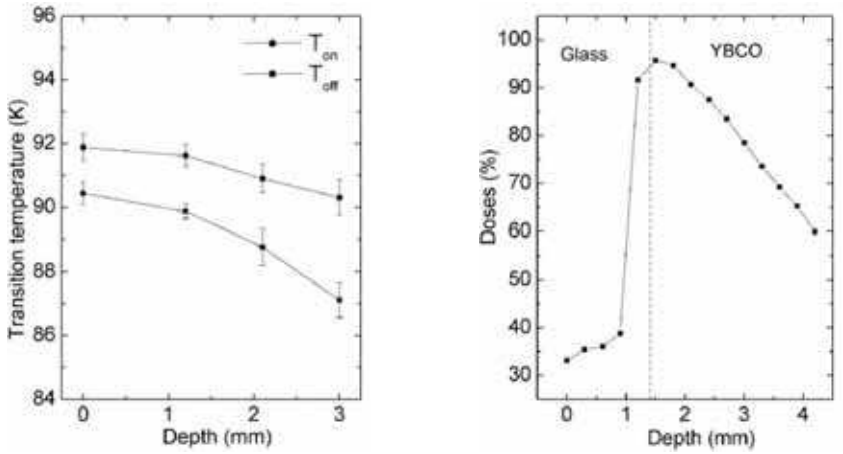

(a) (b)

Fig. 13. (a) In-depth Tc profile in a ^{137}Cs gamma irradiated YBCO sample, Tc measurements were performed through step by step sample polishing. (b) Energy deposition distribution calculated for a model irradiation experiment by means of the EGS-4 code (Leyva et al., 2002a).

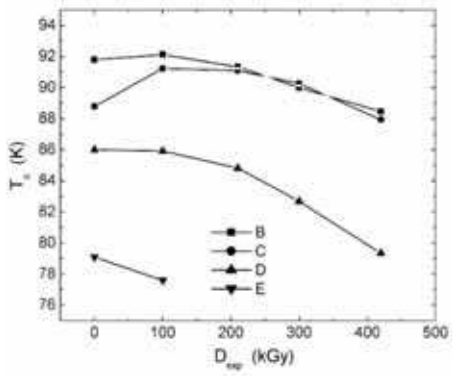

Fig. 14. YBCO superconducting transition temperature Tc dependence on ^{60}Co induced gamma ray exposition doses at different initial non-stoichiometric parameter δ values, 0.05, 0.09, 0.18 and 0.23 for A, B, C and D curves respectively.

6. Gamma radiation damage effects on the YBCO extrinsic properties: critical superconducting electrical current J_c and electrical resistivity

6.1 Critical superconducting electrical current J_c

Independently of the gamma radiation effect over the oxygen random distribution on the basis plane, specially over the Cu(1)-O chain sites, the electronic movement of the Cooper pairs ascribed to the YBCO superconducting properties takes place at the Cu(2)-O_2 planes. Gamma radiation with initial energies $E_\gamma \geq 129$ keV can provoke Oxygen displacements and for $E_\gamma \geq 489$ keV, Cupper displacement, as well, in the Cu(2)-O_2 planes. These effects can be well observed in YBCO thick films exposed to ^{60}Co gamma radiation (Leyva et al, 1995). The electrical resistivity at the normal state shows a nearly linear dependence on the exposition doses, which on the basis of Mathiessen rule, which is expected to be related to a gamma ray induced vacancy concentration upraise in the of the Cu(2)-O_2 planes. In relationship with superconducting transport properties, it had been proved that gamma radiation induces an enhancement of the vortex pinnig energy U_0, as it is shown in Fig. 15a, which should favors transport superconducting properties, like the critical superconducting electrical current J_C.

On the other side, ac susceptibilities superconducting transition measurements had shown that Tc is always over 85 K for the exposition doses up to 500 kGy, with a maximum at $E_0 \approx$ 120 kGy, as was shown pointed out in section 5.2, where in addition a monotonous superconducting volume fraction increasing was also observed (Leyva et al., 2005). However, Fig. 15b shows a J_C monotonous decreasing dependence on the exposition doses, with an inflexion between 150 to 250 kGy, which has been ascribed to the strengthening of the irradiated thick films superconducting properties at E_0, as well as to the vortex pinning energy U_0 upraised showed in Fig. 15a, the last one not being enough to maintain this transitional J_C value at higher exposition doses.

This peculiar J_C suppressing behavior at higher exposition doses, which is radiation damage dependent, seems to be relaying on some extrinsic electrical conduction properties connected with its percolative nature, but independent of atom displacement trials on the Cu(2)-O_2 planes.

In order to get deeper in this picture, ^{57}Co gamma irradiation experiments on YBCO ceramic samples were performed (Mora et al., 1995). Since maximal secondary electron kinetic energy is lower than the electron critical energy for inducing oxygen displacements on Cu(2)-O_2 planes , the atom displacements processes take place only on the Cu(1)-O chains. Fig. 16a shows the J_C dependence on the exposition doses at target temperature of 80 K, where J_C changes very weak under minor oscillatory changes (about 15% amplitude) with the exposition doses, what might be expected under the non occurrence of atom displacements processes at the Cu(2)-O_2 planes in this case.

It seem apparently that by ^{57}Co gamma irradiation on YBCO target cooled at 80 K there not exists any extrinsic effect, as those observed in ^{137}Cs irradiation on YBCO thick film samples. Since vacancy diffusion movements and recombination effects can be neglected at low temperature, it might be expected, that such J_C suppressing mechanism should be even weaker by target irradiation at room temperature. Consequently, the drastic J_C radiation suppressing effect presented in Fig. 16b by target irradiation at room temperature is a surprising one and has been explained by Mora et al. by a radiation conditioned increase of the weak linking Josephson junction thickness *d* (Mora et al., 1995). In Mora et al. model it was taking into the account the influence of the internal magnetic field acting on each superconducting Josephson junction when a critical electrical current fluxes in a

superconducting granular ceramic sample. It was concluded that the weak linking Josephson junction thickness d increase with the exposition doses following approximately a $(D_{exp})^{½}$ law leading to a monotonic J_C diminution with the exposition doses. It is important to note that the irradiated samples in this case showed the Meissner Effect even at exposition doses of 1 kGy, for which no superconducting transition was observed and J_C vanished.

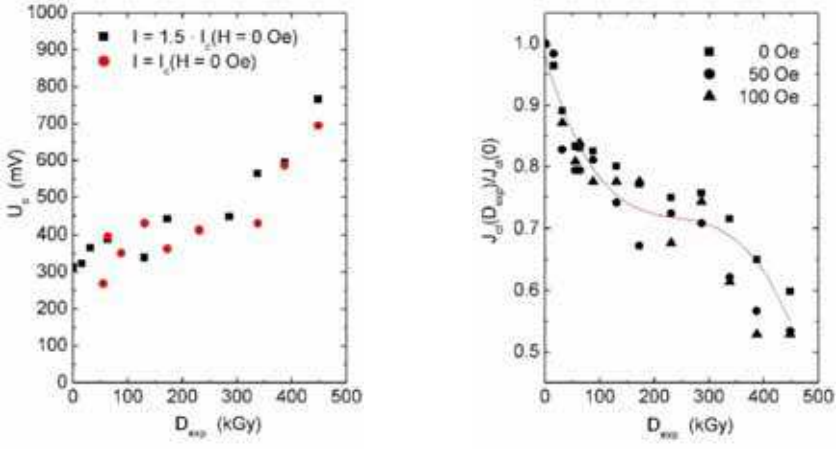

(a) (b)

Fig. 15. Transport properties in a YBCO thick film exposed to ^{60}Co gamma radiation. Vortex pinning energies (a) and superconducting electrical critical current (b) vs. exposition doses; the continuous curve is a visual guide. (Leyva et al, 1995)

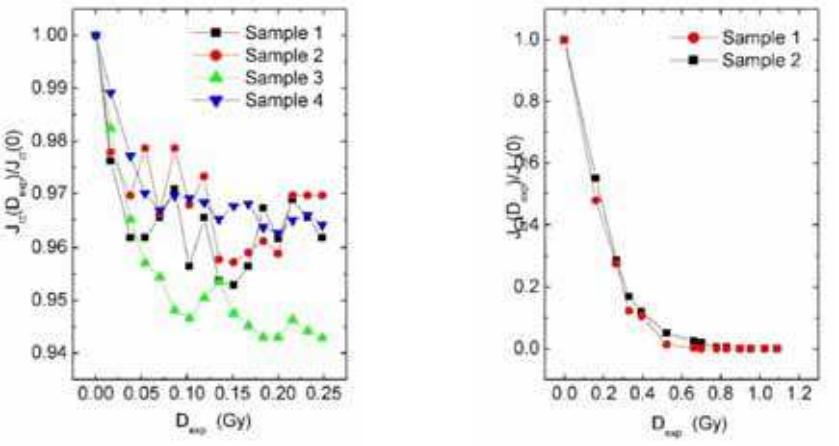

(a) (b)

Fig. 16. Dependence of the superconducting critical current dependence on the ^{57}Co gamma ray exposition doses at different target temperatures: (a) 80 K, (b) 300 K.

Such an exotic electrical conduction behavior have been observed also on regard of the electrical resistivity in the normal state (T > Tc) at relative low ^{57}Co gamma exposition dose,

as it is shown in Fig. 17. Here the electrical resistivity temperature dependence in metallic state has been described according the Mathiessen Law

$$\rho(T, D_{\exp}) = \rho_0(D_{\exp}) + \alpha'(D_{\exp})T \tag{15}$$

where $\rho_0(D_{\exp})$ is the residual electrical resistivity and $\alpha'(D_{\exp})$ is the thermal electrical resistivity coefficient. The Mathiessen Law Eq. (15) is a semiempirical statement which works well in metal and alloys, where ρ_0 has been related to electron elastic scattering processes, as for instance, point crystal defects, and the second term $\alpha'(D_{\exp})T$ represents inelastic electron scattering, like those with lattice phonon. Fig. 17 describes (a) ρ_0 and (b) $\alpha'(D_{\exp})$ dependences with the $D_{\exp}$ in terms of the experiment proportional coefficients $R_0(m\Omega)$ and $\alpha(m\Omega K^{-1})$.

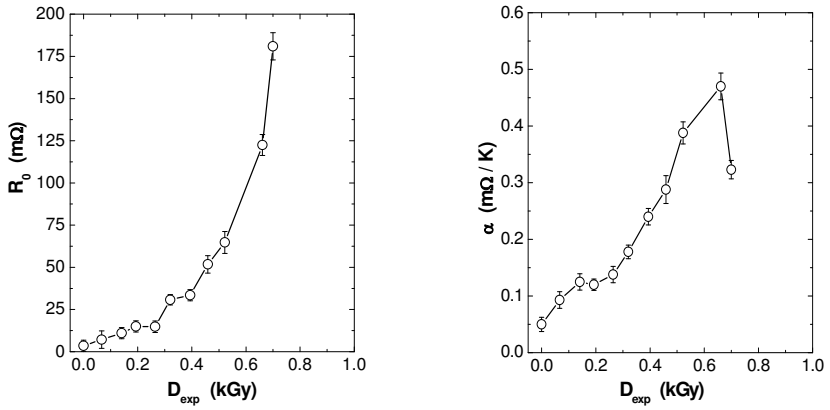

(a) (b)

Fig. 17. Exposition dose dependence of (a) residual resistivity R_0 in (mΩ) and (b) thermal electrical resistivity coefficient α (mΩK^{-1}) of ^{57}Co irradiated YBCO ceramic samples at room temperature.

According to the Mathiessen law, on one side, R_0 must increases proportionally with the exposition doses; on the other side, while α must remain constant, independent from the exposition doses. However, R_0 increases no linearly with the exposition doses, approximately as $1/(E_{MIT}\text{-}D_{exp})$ by approaching to the exposition dose $E_{MIT} \approx 0.7$ kGy, where at the same time α owns a maximum near to E_{MIT}. For $D_{exp} > E_{MIT}$, the samples undergo a kind of metal – insulator transition (at low temperature $T \gtrsim T_c$ semiconducting behavior, while at room temperature metallic one), and finally, at exposition doses higher than 1 kGy, no superconducting transition is observed ($J_C = 0$) and the samples behaves completely as a semiconductor.

Such electrical resistivity dependence with the ^{57}Co gamma exposition doses differs basically form the one corresponding to the ^{60}Co gamma radiation, since in this case, a nearly linear dependence with the exposition doses was observed following well the Mathiessen Law.

6.2 ^{57}Co gamma radiation induced enhanced vacancy diffusive movements in ceramic YBCO samples

The dependence of the Junction Thickness d of the Josephson Weak Linking on the ^{57}Co gamma exposition doses presented by Mora et al. (Mora et al., 1995) was analized taking into the account the following assumptions:

(A) The Junction Thickness d involves the intergrain space with superconductive depleted properties between two neighbour superconductive grains, as well as, the intragrain regions close to the external grain boundaries (GB), which contain high crystalline defects concentration, specially oxygen vacancies, in comparison with the internal intragrain volume defect concentration. This Josephson junction structure is schematically represented in Fig. 18.

(B) During the Gamma irradiation the induced secondary electron shower strongly modify the Activation Energy for intracrystalline oxygen diffusion. Therefore, at a given temperature during irradiation enhanced diffusion motions of atoms and vacancies take place. Due to the high vacancy concentration gradient at GB, the particle diffusive flux is mainly directed inwards to the internal grain regions, where diffusive motions among close YBCO grains can be neglected.

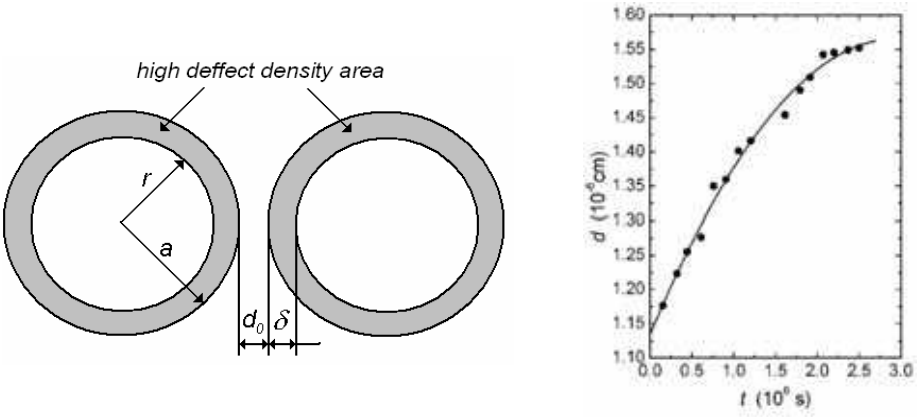

Fig. 18. Schematic representation of the YBCO superconducting weak intergrain linking: intragrain defect distribution and the intergrain junction thickness d (left). Evolution of the superconductive junction thickness d with the ^{57}Co irradiation time (right).

(C) An initial Gaussian Normal Vacancy Distribution, with its maximum value at the Grain Boundary for a supposed typical spherical shaped YBCO´s grain was taken for simplicity, where its thickness $\delta << a$, the grain radius. The Inhomogeneous Diffusion Equation with a constant source term due to Gamma Irradiation induced atomic displacements was applied and solved. Vacancy intergrain diffusion was neglected during irradiation.

From assumptions (A) and (B), following expression of the total Josephson junction thickness d was applied

$$d(t_{irr}) = d_0 + 2\delta(t_{irr}) \tag{16}$$

where d_0 is the intergrain separation (see Fig. 18, left) and the irradiation time was used as a dynamic variable instead of the exposition doses.

Note, that in the present gamma irradiation effect model, main effects arise from the existing high crystal defect concentration at the GB before the irradiation, which will remain higher than the gamma radiation induced crystal defects as a result of oxygen displacements or trapped secondary electrons in oxygen vacancies.
From these calculations it was concluded that $(\Delta d)^2 \propto t_{irr}$, a kind of Einstein's Random Walk dependence. Fig. 18(right) shows the following Mora et al. model calculated Josephson junction thickness d values for the corresponding irradiation times and their fitting according the enhanced vacancy diffusive movement model (Cruz, Leyva & Leyva, 2003). From this fitting the resulting YBCO oxygen vacancy diffusion constant was determined of about 10^{-20} cm/s^2, three orders higher than the value of the Oxygen Diffusion Constant at room temperature for this material at normal conditions. An increase of the Activation Energy of 0.36 eV was also estimated.
The extrapolated value D_{irrad} (77 K) was estimated to be approximately 10^{-60} cm/s^2, showing that on the basis of the mentioned enhanced diffusion mechanism the J_C drastic suppressing effect does not take place when irradiation are made at low temperatures in good agreement with $J_c(D_{exp})$ measured results at target temperature of 80 K (Fig. 16a).
Since gamma radiation damages on Cu(1)-O chain sites are always present due to their low atom displacements threshold energy, the mechanism of J_C drastic suppressing related to gamma radiation induced enhanced vacancy diffusive movements will superpose to other radiation effects taking place at higher gamma ray energies, as was observed in ^{60}Co gamma irradiation experiments presented in Fig. 15 (Leyva et al., 1995).

7. Conclusions

Important improvements have been accomplished recently concerning a detailed description and evaluation of the gamma radiation damage effects in solids, and particularly in high Tc superconductors, were Monte Carlo simulation tools have been introduced in different approaches. In Monte Carlo assisted Classical Method approach, MCCM, the Oen-Holmes-Cahn classical atom displacement rate calculation algorithm was expanded. For this, secondary electron in-depth energy profiles calculated by means of Monte Carlo based codes was introduced, particularly to YBCO superconducting material. On the other side, a new theoretical description of the conditions favoring the occurrence of single fast electron elastic scattering in solids has been developed. Further works in this field are in course, comparing this new atom displacements rate calculation algorithm with previous ones, like MCCM.
On the basis of MCCM approach, gamma quanta induced YBCO in-depth atom displacement rate distributions were calculated up to incident energies lower than 10 MeV. At very low incident energies, oxygen atom displacements take place on Cu(1)-O chain sites. With increasing incident energy, firstly Oxygen displacements in Cu(2)-O_2 planes and other crystalline sites, while at higher energies Cupper displacements are also induced, which begins to be dominant at about 4 MeV and reaches a maximum contribution of 65% at 10 MeV. The corresponding in-depth dpa profiles at different incident energies due to electrons and positrons were characterized as being very similar.
It was concluded, that gamma radiation induced oxygen displacements in both, Cu(2)-O_2 planes and Cu(1)-O chains, as well as secondary electrons are eventually trapped in unoccupied O(4) in Cu(1)-O chain sites in basal planes, favoring oxygen rich nearest neighbor configuration around the Cu(1) sites, provoking a strengthening of the

orthorhombic structural phase properties, specially at relative low exposition dose $E_0 \approx 120$ kGy, depending on the initial non–stiochiometry parameter. In particular, critical temperature enhancement induced by gamma rays at low exposition doses seems to the connected with foregoing changes on the oxygen basal plane disorder.
Electronic transport properties on the Cu(2)-O_2 in the superconducting state are favored by gamma radiation at higher energies, where an strengthening of vortex pinning energies has been observed. However, gamma radiation induces also a the drastic J_C radiation suppressing effect through enhanced vacancy diffusive movements in ceramic YBCO samples, which is sharply temperature dependent and in large scale modulates the supercoducting intergrain boundary properties and its percolative properties.
It may be concluded that gamma radiation induces on high Tc superconductor systhematically crystal structure and superconducting property changes, in a very peculiar way, which deserve future researches in order to get a better understanding of their influence on superconducting mechanisms.

8. References

Abreu, Y.; Cruz, C.M.; Piñera, I. & Leyva, A. (2009). Influencia del desorden cristalino en los espectros Mössbauer del $YBa_2Cu_{3-y}Fe_yO_{7-x}$. *Rev. Cub. Física*, Vol. 26, No. 2A, 179-185, ISSN 0253-9268.

Belevtsev, B.I.; Volchok, I.V.; Dalakova, N.D.; Dotsenko, V.I; Ivanchenko, L.G.; Kuznichenko A.V. & Lagvinov I.I. (2000). Effect of γ-Irradiation on Superconductivity in Polycrystalline $YBa_2Cu_3O_{7-\delta}$. *Phys. Stat. Sol. (a)*, Vol. 181, No. 2, 437-450.

Bethe, H.A. (1953). Molière's Theory of Multiple Scattering. *Phys. Rev.*, Vol. 89, No. 6, 1256-1266.

Bethe, H.A. & J. Ashkin, J. (1953). Passage of Radiations through Matter. In: *Experimental Nuclear Physics*, E. Segré (Ed.), 348, John Wiley & Sons, Inc., New York.

Bohandy, J.; Suter, J.; Kim, B.F.; Moorjani, K. & Adrian, F.J. (1987). Gamma radiation resistance of the high Tc superconductor $YBa_2Cu_3O_{7-\delta}$. *Appl. Phys. Letters*, 51, 25, 2161-2163.

Boiko, B.B.; Korshunov, F.P.; Gatalskii, G.V.; Akimov, A.I.; Gatalskaya, V.I.; Demyanov, S.E. & Stribuk, E.K. (1988). Radiation effect on the superconductivity in the Y-Sm-Ba-Cu-O ceramic system. *Phys. Stat. Sol. (a)*, 107, K139-K144.

Boolchand, P. & McDaniel, D. (1992). Progress in Mössbauer Spectroscopy of High-Temperature Superconductors. *Hyperfine Interactions*, Vol. 72, 125–152.

Bourdillon, A.J. & Tan, N.X. (1995). Displacement damage in supported $YBa_2Cu_3O_{7-x}$ thin films and finite-element simulations. *Supercond. Sci. Technol.*, Vol. 8, No. 7, 507-512.

Briesmeister, J.K. (ed.) (2000). *MCNP™ - A General Monte Carlo N-Particle Transport Code*. Los Alamos National Laboratory Report LA-13709-M, Version 4C.

Cahn, J.H. (1959). Irradiation Damage in Germanium and Silicon due to Electrons and Gamma Rays. *J. Appl. Physics*, Vol. 30, No. 8, 1310-1316.

Cooksey, J.A; Brown, W.D.; Ang, S.S.; Naseem, H.A.; Ulrich, R.K. & West, L. (1994). Gamma-ray and fast neutron radiation effects on thin film superconductors. *IEEE Trans. Nucl. Sci.*, Vol. 41, No. 6, 2521-2524.

Corbett, J.M. (1966). *Electron Radiation Damage in Semiconductors and Metals*, Academic Press, New York and London.

Cruz, C.; Leyva, Y. & Leyva, A. (2003). Ensanchamiento Inducido por la Radiación Gamma de la Frontera de los Granos en Cerámicas Superconductoras. Revista Cubana de Física. Vol. 20, No. 1, 39-43, ISCN: 0253-9268

Cruz, C.; Piñera, I.; Abreu, Y. & Leyva, A. (2008). Theoretical Foundations of Atom Displacements induced by Fast Electron Elastic Scattering in Solids. Proceedings of IEEE Nuclear Sciences Symposium, pp. 2542-2544, ISBN 978-1-4244-2714-7, Dresden, Germany, October 2008, IEEE.

Elkholy, M.M.; El-Deen, L.M.S.; El-Zaidia, M.M., El-Hamalawy, A.A. & Hussain, W.M. (1996). Response of YBCO superconductor doped with strontium after gamma irradiation. *Radiat. Phys. Chem.*, Vol. 47, No. 5, 691-694.

Frischherz, M.C.; Kirk, M.A.; Zhang, J.P. & Weber, H.W. (1993). Transmission electron microscopy of defect cascades in $YBa_2Cu_3O_{7-\delta}$ produced by ion irradiation. *Philosophical Magazine A*, Vol. 67, No. 6, 1347-1363.

Fukuya, K. & Kimura, I. (2003). Calculation of Gamma Induced Displacement Cross-sections of Iron Considering Positron Contribution and Using Standard Damage Model. *J. Nucl. Sci. Technol.*, Vol. 40, No. 6, 423-428.

Gupta, R.P. & Gupta, M. (1991). Order-disorder-driven change in hole concentration and superconductivity in $YBa_2Cu3O_{6.5}$. *Phys. Rev. B*, Vol. 44, No. 6, 2739-2746.

Hendricks, J.S., McKinney, G.W.; Trellue, H.R.; Durkee, J.W.; Finch, J.P.; Fensin, M.L.; James, M.R.; Pelowitz, D.B.; Waters, L.S.; Gallmeier, F.X. & David, J.C. (2006). *MCNPX™ Version 2.6.B*, Los Alamos National Laboratory report, LA-UR-06-3248 (June 2006).

JCPDS - Join Committee of Powder Diffraction Studies (1993). *Inorganic Index to the Powder Diffraction File*, 38-1433.

Jin, M.Z.; Liu, X.W.; Liu, M.L.; Xu, J.; Liu, R. & Jia, Y.Q. (1997). Mössbauer spectra of ^{57}Fe in thick film of $YBa_2(Cu_{0.97}Fe_{0.03})_3O_{7-x}$ irradiated by a large dose of γ-rays. *Physica C*, Vol. 288, 226-230.

Kawrakow, I. & Rogers, D.W.O. (2003). The EGSnrc Code System: Monte Carlo Simulation of Electron and Photon Transport. *NRCC Report* PIRS-701, Dec. Stanford Univ., California.

Kinchin, G.H. & Pease, R.S. (1955). The Displacement of Atoms in Solids by Radiation. *Rep. Prog. Phys.*, Vol. 18, 1-51.

Kirk, M.A.; Baker, M.C.; Lin, J.Z.; Lam, D.J. & Weber, H.W. (1988). Defect structures in $YBa_2Cu_3O_{7-x}$ produced by electron irradiation. In: *High Temperature Superconductors*, Brodsky, M.B.; Dynes, R.C.; Kitazawa, K. & Tuller, H.L. (Eds.), 209, MRS Symposia Proceedings No. 99, Material Research Society, Pittsburg.

Kirk, M.A. & Yan, Y. (1999). Structure and properties of irradiation defects in $YBa_2Cu_3O_{7-x}$. *Micron*, Vol. 30, 507-526.

Klein, O. & Nishina, Y. (1929). Über die Streuung von Strahlung durch freie Elektronen nach der neuen relativistischen Quantendynamik von Dirac. Zeitschrift für Physik A Hadrons and Nuclei, Vol. 52, No. 11-12, 853-868.

Lancaster, G. (1973). *Paramagnetische Elektronen Resonanz in Halbleitern*, Akademische Verlagsgesellschaft, Geest & Portig, Leipzig, Germany.

Legris, A.; Rullier-Albenque, F.; Radeva, E. & Lejay, P. (1993). Effects of electron irradiation on $YBa_2Cu_30_{7-\delta}$ superconductor. *J. Phys. I France*, Vol. 3, No. 7, 1605-1616.

Leyva, A.; Suárez, J.C.; Mora, M.; Cruz, C.M. & Quesada, D. (1992). AC Magnetic Susceptibility in High Temperature Superconductors Irradiated with γ-Rays. *Phys. Stat. Sol. (a)*, Vol. 134, No. 1, K29-K31.

Leyva, A.; Mora, M.; Martin, G. & Martinez, A. (1995). Irradiation effect of Co-60 gamma rays in YBCO thick films. Supercond. Sci. Technol., Vol. 8, No. 11, 816-821.

Leyva, A. (2002). Efectos de las radiaciones gammas en cerámicas superconductoras de interés en las tecnologías nucleares. PhD Thesis on Physics, University of Havana.

Leyva, A.; Alfonso, A. & Cruz, C. (2002). Transition temperature depth profiling of Cs^{137} gamma-irradiated YBCO ceramic. *Nucl. Instr. and Meth. B*, Vol. 174, No. 1-2, 222-224.

Leyva, A.; Cruz, C.M.; Mora, M.; Shtejer, K.; Diez, J.C.; Angurel, L.A.; Piñera, I. & Abreu, Y. (2005). The effects of ^{137}Cs and ^{60}Co γ radiation on the magnetic susceptibility of BSCCO textured thin rods. *Nucl. Instr. and Meth. B*, Vol. 239, No. 3, 281-285.

Liu, Y.H.; Che, G.C.; Li, K.Q. & Zhao, Z.X. (2005). Superconductivity and Mössbauer effect of $Fe_xCu_{1-x}Ba_2YCu_2O_{7-y}$ superconductors synthesized by high pressure. *Phys. Rev. B*, Vol. 71, 104503.

Lyubutin, I.S.; Terziev, V.G. & Dmitrieva, T.V. (1989). Lattice sum calculations and electric field gradients for orthorhombic and tetragonal phases of $YBa_2Cu_3O_x$. *Physics Letter A*, Vol. 137, No. 3, 144-148.

McKinley, W.A. & Feshbach, H. (1948). The Coulomb Scattering of Relativistic Electrons by Nuclei. Phys. Rev., Vol. 74, No. 12, 1759-1763.

Mora, M.; Cruz, C.M.; Leyva, A.; Suárez, J.C.; & Quesada, D. (1995). Influencia de la radiación γ del Co-57 sobre las uniones débiles intergranulares de las cerámicas superconductoras YBCO. *Nucleus*, Vol. 18, 21-24.

Mott, N.F. & Massey, H.S.W. (1952). *The Theory of Atomic Collisions*, 2nd Edition, Oxford University Press, England.

Nelson, W.R.; Hrayama, H.H. & Rogers, D.W.O. (1985). *The EGS-4 Code System*, SLAC-Report-225, Dec. Stanford Univ., California.

Oen, O.S. & Holmes, D.K. (1959). Cross Sections for Atomic Displacements in Solids by Gamma Rays. J. Appl. Phys., Vol. 30, No. 8, 1289-1295.

Piñera, I. (2006). Estudio del Daño Radiacional en materiales sólidos mediante la simulación de procesos físicos. Master Degree These on Nuclear Physics. High Institute on Technologies and Applied Sciences, InTEC, Havana City, December 2006.

Piñera, I.; Cruz, C. ; Abreu, Y. & Leyva, A. (2007a). Determination of Atom Displacements Distribution on YBCO superconductor induced by Gamma Radiation. *Phys. Stat. Sol. (a)*, Vol. 204, No. 7, 2279-2286.

Piñera, I.; Cruz, C.; Leyva, A. & Abreu, Y. (2007b). Displacement per atom calculation in YBCO superconductors through Monte Carlo simulation. *Nucl. Instrum. Meth. B*, Vol. 265, No. 2, 536-540.

Piñera, I.; Cruz, C.; Abreu, Y. & Leyva, A. (2008a). Monte Carlo simulation study of positron contribution to displacement per atom production in YBCO superconductors. *Nucl. Instr. and Meth. B*, Vol. 266, No. 22, 4899-4902.

Piñera, I.; Cruz, C.; Abreu, Y. ; Leyva, A.; Cabal, A.E. & Van Espen, P. (2008b). Monte Carlo Assisted Classical Method for the Calculation of *dpa* Distributions in Solid Materials. *Proceedings of IEEE Nuclear Sciences Symposium*, pp. 2557-2560, ISBN 978-1-4244-2714-7, Dresden, Germany, October 2008, IEEE.

Polyak, O.Yu.; Tukhvatulin, R.Kh.; Chan, K.G.; Gasanov, E.M. & Ibragimova, E.M. (1990). Effect of γ-Irradiation on $YBa_2Cu_3O_{7-x}$ Ceramics and Monocrystals in the Superconducting State. *Phys. Stat. Sol. (a)*, Vol. 122, No. 1, K45-K50.

Santoro, A. (1991). *Chemistry of Superconductor Materials,* Noyes Publications, Park Ridge, New Jersey, USA.

Sarkar, M.; Patel, N.V.; Mehta, P.K. & Somayajulu, R.S. (2001). Mössbauer Study of Multiple Substitutions in YBCO. *Hyperfine Interactions*, Vol. 136-137, 587-592.

Thomas, B.S.; Marks, N.A.; Corrales, L.R. & Devanathan, R. (2005). Threshold displacement energies in rutile TiO_2: A molecular dynamics simulation study. *Nucl. Instrum. Meth. B*, Vol. 239, No. 3, 191-201.

Vašek, P.; Smrčka, L.; Dominec, J.; Pešek, M.; Smrčková, O. & Sýkorová, D. (1989). Gamma irradiation of $YBa_{2Cu3O7-x}$ ceramics. Solid State Commun., Vol. 69, No. 1, 23-25.

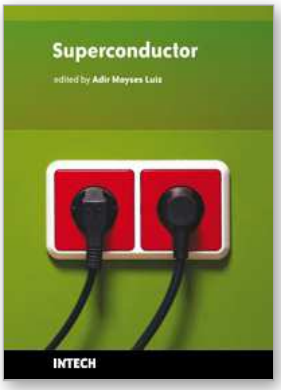

Superconductor

Edited by Doctor Adir Moyses Luiz

ISBN 978-953-307-107-7
Hard cover, 344 pages
Publisher Sciyo
Published online 18, August, 2010
Published in print edition August, 2010

This book contains a collection of works intended to study theoretical and experimental aspects of superconductivity. Here you will find interesting reports on low-Tc superconductors (materials with Tc< 30 K), as well as a great number of researches on high-Tc superconductors (materials with Tc> 30 K). Certainly this book will be useful to encourage further experimental and theoretical researches in superconducting materials.

How to reference

In order to correctly reference this scholarly work, feel free to copy and paste the following:

Carlos M. Cruz Inclán, Ibrahin Pinera Hernandez, Antonio Leyva Fabelo and Yamiel Abreu Alfonso (2010). Studies on the Gamma Radiation Responses of High Tc Superconductors, Superconductor, Doctor Adir Moyses Luiz (Ed.), ISBN: 978-953-307-107-7, InTech, Available from: http://www.intechopen.com/books/superconductor/studies-on-the-gamma-radiation-responses-of-high-tc-superconductors

INTECH
open science | open minds

InTech Europe
University Campus STeP Ri
Slavka Krautzeka 83/A
51000 Rijeka, Croatia
Phone: +385 (51) 770 447
Fax: +385 (51) 686 166
www.intechopen.com

InTech China
Unit 405, Office Block, Hotel Equatorial Shanghai
No.65, Yan An Road (West), Shanghai, 200040, China
中国上海市延安西路65号上海国际贵都大饭店办公楼405单元
Phone: +86-21-62489820
Fax: +86-21-62489821